Fluorinated SiO_2 nanoparticle size effect on traffic marking coatings

Hua Yang[1], Zetong Feng[2]
[1]Jiangxi Transport Investment Consulting Group Co., Ltd., Nanchang, Jiangxi, 330038, China
[2]School of Materials Science and Engineering, Chang'an University, Xi'an, 710018, China
[2]Corresponding author
E-mail: [1]*yanghua0243@163.com*, [2]*17829271288@163.com*

Received 26 June 2026; accepted 8 September 2026; published online 1 November 2026
DOI https://doi.org/10.21595/vp.2026.26782

78th International Conference on Vibroengineering in Lviv, Ukraine, October 1, 2026

Copyright © 2026 Hua Yang, et al. This is an open access article distributed under the Creative Commons Attribution License, which permits unrestricted use, distribution, and reproduction in any medium, provided the original work is properly cited.

Abstract. Under rainwater and mechanical abrasion, traffic markings undergo rapid visibility loss, raising critical transportation safety concerns. From a materials engineering standpoint, fluorinated SiO_2 nanoparticles (F-SiO_2) of five sizes (20 nm to 1000 nm) were incorporated into a marking coating. Standardized Taber abrasion testing was employed to investigate the particle-size dependence of wetting, saline corrosion resistance, and wear-induced hydrophobic evolution. The 50 nm particles created an optimal micro/nano morphology that sustained a Cassie–Baxter state (water contact angle > 150°, sliding angle < 5°). During Taber abrasion, preferential matrix wear progressively exposed the embedded particles; the well-matched micro/nano scales of the 50 nm filler enabled synergistic regeneration of surface chemistry and topography. After 200 cycles, the coating maintained a contact angle > 150° and a sliding angle < 5°, with mass loss reduced by over 80 % relative to a pure coating and virtually no decline in superhydrophobicity. In contrast, 20 nm particles were easily encapsulated and lacked long-term wear resistance, while particles ≥ 100 nm induced an irreversible Wenzel transition. This particle-size window therefore combines wear-induced hydrophobic regeneration with saline corrosion resistance, providing a basis for long-life, maintenance-free self-cleaning traffic markings.

Keywords: traffic marking, fluorine-modified nanoparticles, particle size, Taber abrasion, mechanical durability.

1. Introduction

Wet retroreflectivity loss in traffic markings poses nighttime safety hazards. Superhydrophobic self-cleaning coatings can restore retroreflectivity by shedding water films [1], but wear-induced microstructural damage severely limits durability [2]. Recent investigations have established a comprehensive understanding of this degradation-regeneration cycle: Lu et al. [3] identified that abrasion simultaneously collapses the hierarchical roughness and triggers photocatalytic oxidation of fluorinated groups, yet confined PDMS photocatalysis can balance contaminant degradation with hydrophobic self-healing; Wei [4] further demonstrated that optimally sized nanoparticles construct a self-similar three-tier architecture, enabling worn surfaces to expose fresh layers with nearly identical topography and chemistry; Wu et al. [5] complemented these findings by revealing that mechanical abrasion combined with UV irradiation synergistically reconstructs hierarchical roughness – abrasion exposes embedded fillers while UV degrades residual resin – to enhance air entrapment and restore the Cassie-Baxter state. F-SiO_2 with low surface energy and tunable topology are promising building blocks, yet the role of particle size in wetting and wear resistance remains poorly understood [6]. Abrasion can preferentially remove the resin matrix, exposing embedded F-SiO_2 and regenerating -CF_3/-CF_2- groups [7]. If the exposed particle packing sustains a Cassie-Baxter state, hydrophobicity can dynamically recover [8]. This particle-size-dependent regeneration mechanism relies on in-situ particle retention and roughness regeneration, both governed by particle size [9].

In the context of transportation engineering, the abrasive action of vehicle tires and road debris

necessitates a thorough mechanical evaluation of these functional coatings. This study systematically investigates five sizes of F-SiO_2 in a traffic marking coating. In addition to chemical and morphological characterization, special emphasis is placed on standardized mechanical abrasion testing to bridge the gap between laboratory findings and field performance. The objectives are to reveal the regulatory roles of particle size in wetting state and wear resistance, to verify the feasibility of the abrasion-induced hydrophobicity recovery mechanism, and to define a particle size window for durable self-cleaning traffic markings.

2. Materials and methods

2.1. Materials

FEVE fluorocarbon resin was supplied by Nanjing Wanqing Chemical and Glass Instrument Co., Ltd. Leveling agent (TEGO 450), dispersant (KP110), and anti-settling agent (BYK410) were purchased from Shanghai Deyude Co., Ltd. Rutile titanium dioxide (TiO_2, 1500 mesh, analytical grade), rutile nano-titanium dioxide (Nano-TiO_2, average particle size 20 nm, analytical grade), and ground calcium carbonate ($CaCO_3$, 400, 800, and 1000 mesh, purity 98 %) were purchased from Shandong Yousuofu Chemical Technology Co., Ltd. Polydimethylsiloxane (PDMS, DC 184) was provided by Tianjin Youheng Electronic Technology Co., Ltd. Nano-silica (Nano-SiO_2, average particle sizes of 20, 50, 100, 500 and 1000 nm, analytical grade) and perfluorodecyltriethoxysilane (PFDTES, analytical grade) were obtained from Aladdin Reagent (Shanghai) Co., Ltd. Benzoyl peroxide (BPO, purity 98 %) was purchased from Shandong Yousuofu Chemical Technology Co., Ltd. All reagents were used as received without further purification.

2.2. Preparation of road marking coatings

F-SiO_2 was prepared by reacting SiO_2 with perfluorodecyltriethoxysilane (PFDTES) in ethanol using ammonia as catalyst at 60 °C for 24 h. For the coating, FEVE resin was first mixed with PDMS and additives (dispersant, anti-settling, leveling agent). A pre-dispersed slurry of F-SiO_2 (3 g), nano-TiO_2, rutile TiO_2, and $CaCO_3$ was then incorporated under high-speed stirring. The mixture was blade-coated onto cement mortar substrates and cured at 50 °C for 2 h, yielding samples designated F-20 to F-1000 according to the F-SiO_2 particle size.

2.3. Wettability and morphology characterization

Fourier transform infrared spectroscopy (FTIR, Thermo Fisher Nicolet iS20, USA) was used to characterize the SiO_2 before and after modification over 400-4000 cm^{-1}. Surface morphology was observed with field emission scanning electron microscopy (SEM, ZEISS Sigma 360, Germany).

Static and dynamic wettability were evaluated using an optical contact angle goniometer (KRÜSS DSA 100, Germany). A 5 μL deionized water droplet was dispensed onto the coating at 25 °C. The static water contact angle (WCA) was obtained by fitting the profile with the Young-Laplace equation. The sliding angle (SA) was recorded by tilting the sample stage at a slow rate until the droplet began to roll off.

2.4. Taber abrasion test

The wear resistance of the coatings was assessed using a Taber-type rotary platform abraser (JM-V, China) in accordance with JT/T 995-2015. Coated cement mortar specimens (100 mm×100 mm×5 mm) were fixed on a turntable rotating at 200 $r \cdot min^{-1}$. A pair of CS-10 resilient rubber abrasive wheels, each loaded with 1000 g, were applied to the coating surface. The test was conducted at 25 °C and 50 % relative humidity. After every 40 cycles, the specimens

were removed, cleaned with compressed air, and weighed on an analytical balance (0.1 mg readability) to determine mass loss. The WCA and SA were re-measured at the same intervals.

3. Results and discussion

3.1. Characterization of F-SiO_2

The FTIR spectra of pristine nano-SiO_2 and F-SiO_2 are compared in Fig. 1. In the spectrum of pristine SiO_2, the broad absorption band near 3440 cm^{-1} is attributed to the stretching vibrations of surface silanol groups (Si-OH) and O-H in physically adsorbed water. The peak at 1635 cm^{-1} corresponds to the H-O-H bending vibration. The strongest peak at 1105 cm^{-1} is assigned to the Si-O-Si asymmetric stretching vibration. The band at 802 cm^{-1} is associated with the Si-O-Si bending vibration, and the weak peak at 966 cm^{-1} belongs to the in-plane bending vibration of Si-OH. After modification with PFDTES, the spectrum of F-SiO_2 changed significantly. New absorption peaks appeared at 2927 cm^{-1} and 2856 cm^{-1}, which are attributed to the asymmetric and symmetric stretching vibrations of the ethylene segments (-CH_2CH_2-) in the perfluorodecyl chains. A group of shoulder peaks emerged near 1209 cm^{-1}, characteristic of the C-F stretching vibrations in the perfluorocarbon chains. Meanwhile, the O-H stretching vibration peak near 3440 cm^{-1} weakened markedly and narrowed, indicating that most surface silanol groups on SiO_2 participated in the condensation reaction. Furthermore, the Si-O-Si asymmetric stretching peak at 1105 cm^{-1} broadened and intensified significantly, confirming that new Si-O-Si covalent bonds formed through condensation between hydrolyzed PFDTES and surface silanol groups. These spectral changes confirm that PFDTES was successfully grafted onto the SiO_2 surface via covalent bonding.

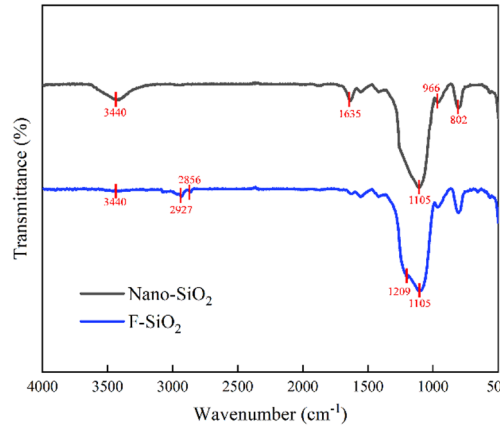
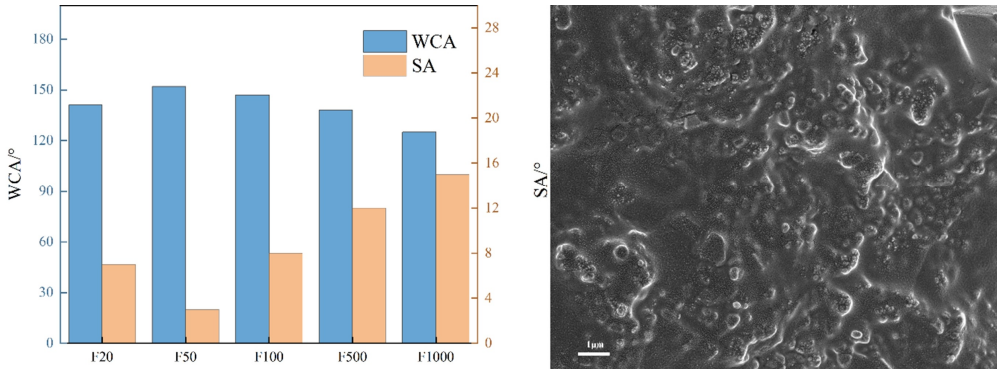


Fig. 1. FTIR spectra of nano-SiO_2 and F-SiO_2

3.2. Wettability

Fig. 2(a) shows that the WCA and SA of F-SiO_2 coatings exhibit a non-monotonic trend with particle size. The optimum is achieved at 50 nm (WCA 152°, SA 3°), where the particles form a uniform micro/nano composite morphology (Fig. 2(b)) that stably sustains a Cassie–Baxter state. As particle size increases further, hydrophobicity degrades progressively: F-100 (WCA 148°, SA 8°) signals early Cassie-state deterioration, F-500 (WCA 138°, SA 22°) indicates partial wetting, and F-1000 (WCA 125°, SA 35°) essentially transitions to the Wenzel state, as larger inter-protrusion spacing fails to seal air cushions. Conversely, the smaller 20 nm particles do not enhance hydrophobicity (WCA 141°, SA 18°); their easy encapsulation by the resin reduces effective surface roughness. Thus, superhydrophobicity is not a monotonic function of particle

size but depends on the balance between particle exposure and roughness configuration, with ~50 nm being the optimal window.



a) b)

Fig. 2. a) Comparison of WCA and SA for F-SiO_2 coatings with different particle sizes; b) SEM image of the F-50 coating surface

3.3. Abrasion resistance stability

The abrasion resistance stability of the coatings – defined here as their capacity to retain hydrophobicity and limit mass loss under repeated mechanical wear – was evaluated through Taber abrasion over 200 cycles [10]. The pure coating exhibited extremely poor stability: after only 40 cycles, it became completely hydrophilic (WCA = 68°) and lost 14.7 mg of mass. In sharp contrast, the F-50 coating demonstrated outstanding abrasion stability. Even after the full 200 cycles, it preserved a superhydrophobic state (WCA = 151°, SA = 4°) with a mass loss of merely 2.9 mg, equivalent to an 80.3 % reduction compared to the 40-cycle loss of the neat coating. This exceptional stability originates from the preferential removal of the softer resin matrix, which continuously uncovers embedded 50 nm F-SiO_2 particles. The exposed particles then form a load-bearing micro-texture that regenerates low-surface-energy $–CF_x$ groups and sustains a Cassie-Baxter air cushion, effectively transforming the wear mode from severe adhesive wear of the pure resin into mild particle-reinforced abrasion. This self-renewal mechanism is key to long-term wear stability.

The 20 nm coating exhibited a moderate improvement in hydrophobicity after 200 cycles (WCA from 141° to 147°, SA from 18° to 13°), confirming that matrix removal does expose fluorinated particles. However, its wear stability was compromised by easy particle pull-out, which resulted in a higher mass loss of 5.4 mg and prevented the formation of a fully stable Cassie-state air cushion. For coatings with larger particles (F-100 to F-1000), the abrasion stability deteriorated substantially. WCA decreased progressively from 144° to 131°, and further to 118°~116°, while mass loss increased from 4.6 mg to as high as 12.1 mg. Here, the wide inter-particle spacing could no longer support a stable Cassie state, and the protruding large particles acted as stress concentrators, causing matrix cracking, accelerated particle detachment, and an irreversible transition to the Wenzel state. Consequently, these coatings suffered a permanent loss of hydrophobicity and high wear rates.

Overall, the 50 nm F-SiO_2 filler provides the best abrasion resistance stability by simultaneously optimizing matrix wear kinetics, particle retention, and topographic regeneration. This synergy minimizes mass loss, preserves a Cassie-Baxter state under prolonged wear, and establishes a clear mechanical design rule for long-life, maintenance-free traffic markings. Table 1 compares the self-repair mechanisms and durability performance of four representative superhydrophobic coating systems. Specifically, the system based on abrasion-induced regeneration of low surface energy (No. 1) exhibits a mass loss of only 2.9 mg after 200 abrasion

ISSN PRINT 2345-0533, ISSN ONLINE 2538-8479

cycles, with the water contact angle decreasing slightly from 152° to 151°, demonstrating excellent mechanical stability. In contrast, the self-similar structure with micro-armor protection (No. 4) possesses an initial contact angle as high as 165.1°, which remains above 150° after 100 Taber abrasion cycles or 150 tape-peeling cycles, indicating the best retention of superamphiphobicity. By comparison, the UV-assisted synergistic recovery systems (No. 2 and No. 3) show decreased hydrophobicity or limited cycle numbers under purely mechanical abrasion; however, after combined abrasion and UV treatment, their contact angles can recover and even increase to 155-160°. In particular, No. 3 retains 87.6 % of its hydrophobicity after 40 abrasion cycles, revealing notable stimulus-responsive self-repair potential. Overall, No. 1 and No. 4 are more advantageous for long-term mechanical durability, while No. 2 and No. 3 are distinguished by their repairability and enhancement of hydrophobicity. Compared with similar systems reported in the literature, the low mass loss of No. 1 and the high contact-angle retention of No. 4 are both at a superior level.

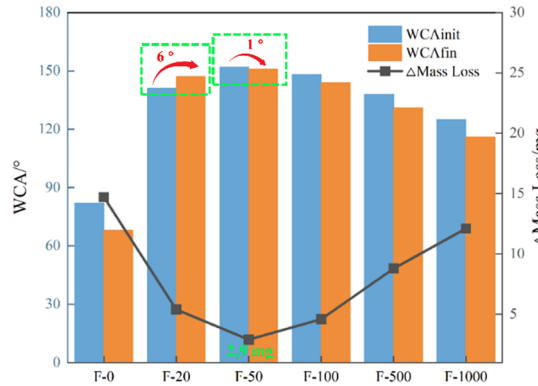


Fig. 3. WCA and Mass Loss of F-SiO_2 coatings with different particle sizes before and after abrasion

Table 1. Comparison of self-repair mechanisms and durability performance of representative superhydrophobic coating systems

No.	Source	Mechanism	Initial WCA	Treatment	Durability indicator	Result
1	This article	Abrasion-induced low-surface-energy regeneration	152°	200 abrasion cycles	Mass loss: 2.9 mg	WCA: 151°
2	[3]	Mechanical-UV synergistic hierarchical texturing	124°	200 abrasion cycles	Mass loss: 24 mg (abrasion only); 6 mg (abrasion + UV)	WCA: 138° (after abrasion); 160° (after abrasion + UV)
3	[5]	UV-PDMS synergistic hydrophobic recovery	145°	40 abrasion cycles	Luminance factor retention: 86.6 % (20 cycles) / 80.3 % (40 cycles)	Hydrophobicity retention: 87.6 %; WCA recovered and increased to 155° after abrasion + UV
4	[4]	Self-similar structure with micro-armor protection	165.1°	100 Taber abrasion cycles or 150 tape peeling cycles	–	WCA remained > 150° (superamphiphobicity maintained)

3.4. Saline-resistant stability

To assess saline corrosion resistance, coatings were immersed in 3.5 wt% NaCl at 25 °C for 72 h. All F-SiO_2 coatings retained high hydrophobicity with WCA drops below 10°, confirming

the chemical inertness of the fluorocarbon matrix. The F-50 coating exhibited the smallest decline (152° to 149°) with virtually unchanged SA, as its stable Cassie-Baxter state prevents saline solution penetration and confines salt crystallization to outermost asperities. Coatings with 20 nm or larger particles showed slightly greater WCA decreases due to less robust air cushion sealing. Thus, the 50 nm F-SiO_2 filler combines optimal wear-induced hydrophobic regeneration with superior saline corrosion resistance, reinforcing its potential for durable self-cleaning traffic markings (Fig. 4).

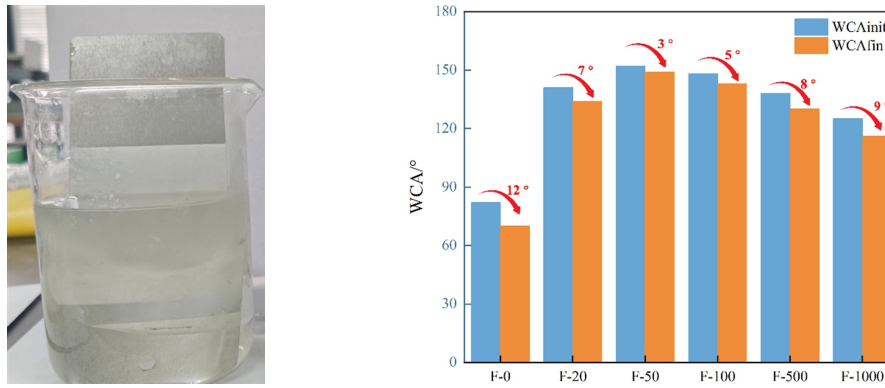


Fig. 4. a) Immersion of the coatings in NaCl solution b) WCA changes of different groups before and after immersion

4. Conclusions

1) Hydrophobicity peaks at 50 nm (WCA 152°, SA 3°) due to optimal particle exposure and roughness. Smaller particles are easily encapsulated; larger ones fail to sustain the Cassie state.

2) Under Taber abrasion (200 cycles), the 50 nm filler retains superhydrophobicity (WCA 151°, SA 4°) and reduces mass loss by 80.3 % through synergistic matrix removal, particle retention and topography renewal. Particles ≤ 20 nm suffer from pull-out, while those ≥ 100 nm cause stress-concentration cracking and irreversible Wenzel degradation.

3) The 50 nm F-SiO_2 filler thus converts mechanical abrasion into a surface self-renewal driving force, offering a mechanical design rule for long-life self-cleaning traffic markings.

Acknowledgements

Special thanks go to the laboratory staff at Chang'an University for their support in data collection and experimental setup. This work was financially supported by the Science and Technology Project of the Department of Transportation of Jiangxi Province (Grant No. 2021H0034).

Data availability

The datasets generated during and/or analyzed during the current study are available from the corresponding author on reasonable request.

Conflict of interest

The authors declare that they have no conflict of interest.

ISSN PRINT 2345-0533, ISSN ONLINE 2538-8479

References

[1] Y. Yang, H. He, Y. Li, and J. Qiu, "Using nanoimprint lithography to create robust, buoyant, superhydrophobic PVB/SiO2 coatings on wood surfaces inspired by red roses petal," *Scientific Reports*, Vol. 9, No. 1, p. 9961, 2019, https://doi.org/10.1038/s41598-019-46337-y

[2] Q. F. Xu, J. N. Wang, and K. D. Sanderson, "Organic−inorganic composite nanocoatings with superhydrophobicity, good transparency, and thermal stability," *ACS Nano*, Vol. 4, No. 4, pp. 2201–2209, Apr. 2010, https://doi.org/10.1021/nn901581j

[3] X. Lu, H. Wu, L. Li, R. He, and H. Guo, "Confined photocatalysis and interfacial reconstruction for durability wettability in road markings," *Colloids and Surfaces A: Physicochemical and Engineering Aspects*, Vol. 729, p. 138902, Nov. 2025, https://doi.org/10.1016/j.colsurfa.2025.138902

[4] J. F. Wei, "Preparation and properties of durable superhydrophobic/superamphiphobic coatings," (in Chinese), *Lanzhou University of Technology*, 2024, https://doi.org/10.27206/d.cnki.ggsgu.2024.000015

[5] H. Wu, X. Lu, Z. Feng, and R. He, "Dynamic hydrophobicity and surface reconstruction mechanism of self-cleaning traffic marking coatings incorporating modified TiO2 nanoparticles," *Construction and Building Materials*, Vol. 497, p. 143876, 2025, https://doi.org/10.1016/j.conbuildmat.2025.143876

[6] J.-D. Brassard, D. K. Sarkar, and J. Perron, "Synthesis of monodisperse fluorinated silica nanoparticles and their superhydrophobic thin films," *ACS Applied Materials and Interfaces*, Vol. 3, No. 9, pp. 3583–3588, 2011, https://doi.org/10.1021/am2007917

[7] Y. Wu et al., "Facile spraying fabrication of highly flexible and mechanically robust superhydrophobic F-SiO2@PDMS coatings for self-cleaning and drag-reduction applications," *New Journal of Chemistry*, Vol. 42, No. 22, pp. 18208–18216, 2018, https://doi.org/10.1039/c8nj04275f

[8] S. M. Mirabedini, F. Zareanshahraki, and V. Mannari, "Enhancing thermoplastic road-marking paints performance using sustainable rosin ester," *Progress in Organic Coatings*, Vol. 139, p. 105454, Nov. 2019, https://doi.org/10.1016/j.porgcoat.2019.105454

[9] J. Nance and T. D. Sparks, "From streetlights to phosphors: a review on the visibility of roadway markings," *Progress in Organic Coatings*, Vol. 148, p. 105749, Jun. 2020, https://doi.org/10.1016/j.porgcoat.2020.105749

[10] D. Wang et al., "A novel method for evaluating the durability and environmental pollution of road markings on asphalt pavement," *Journal of Cleaner Production*, Vol. 411, p. 137255, Apr. 2023, https://doi.org/10.1016/j.jclepro.2023.137255